Modeling of hourly and daily values of erythemal ultraviolet radiation in Santiago de Chile City

Lisdelys González-Rodríguez[1], Jorge Rosas[2], Amauri Pereira de Oliveira[2], Lien Rodríguez[3], David Contreras[4] and Carolina Baeza[3]

[1] Engineering Faculty/University of Concepcion, Concepcion (Chile)
[2] Institute of Astronomy, Geophysics and Atmospheric Science/University of São Paulo, São Paulo (Brazil)
[3] Eula Center, Environmental Science Faculty/University of Concepcion, Concepción (Chile)
[4] Biotechnology Center/University of Concepcion, Concepcion (Chile)

Abstract

Ultraviolet radiation is an important and highly energetic component of solar spectrum that needs to be monitored because is harmful to life on Earth, especially in areas where ozone layer has been depleted like Chile. The erythemal ultraviolet (UVER) radiation, corresponding to 280-315 nm, is the component of ultraviolet band most used to identify overexposure limits. In this work, four years of UVER measurements at the surface, carried out from January 1st, 2015 to December 31th, 2018, in Santiago City, Chile, are analyzed and used to develop a mathematical regression models to estimate UVER in terms of solar global irradiance (IG). The UVER models, obtained by fitting a second-degree polynomial, perform better during summer (RMSE=0.028, NRMSE=20%) and the worst in the winter (RMSE=0.015, NRMSE=54%) for hourly values. Similarly, performance is presented by daily values of UVER.

Keywords: solar global irradiance, erythemal ultraviolet UVER, Chile

1. Introduction

Ultraviolet radiation (UV) is a highly energetic component of solar spectrum that needs to be monitored because is harmful to life on the Earth, especially in areas where the ozone layer has been depleted like Chile (Rivas and Rojas, 2018). It is subdivided into three specific bands: UV-A: $320<\lambda<400$nm; UV-B: $280<\lambda<320$nm; UV-C: $200<\lambda<280$nm. The UV-C is completely absorbed by the ozone layer; however, a significant fraction of UV-B and UV-A reach the surface. Human, animals, plants and materials can be negatively affected by the radiation within these spectral bandwidths. Human overexposure to solar UV-B radiation is properly identified through ultraviolet erythemal radiation at the surface (UVER, 280-315 nm), which is determined by the integral of the UV-B power spectrum weighted by the erythemal action spectrum given by the CIE (Commission Internationale de l'Éclairage) (McKinlay, A.F. and Diffey, 1987). The erythema action spectrum and UVER are the basis of UV index (UVI), which is used globally for public health risk information. Examples of UVER negatives effects in human beings are reddening of the skin (erythema), reduction of vitamin-D synthesis, cataracts, suppression of the immune system and developing of skin cancer and melanoma (Rivas et al., 2014). Melanoma is the first cause of death among skin diseases, a malignant and very aggressive skin cancer. Worldwide, melanoma is responsible for 59,782 global deaths (Karimkhani et al., 2017). In Chile, according to the Chilean Society of Dermatology, 237 people die from skin cancer every year (Hartman and Calvo, 2014). In this country, during the period 2010-2015, there was an 20 % increase in the number of skin cancer cases, affecting mainly elderly persons (Iribarren B. et al., 2018). Santiago, which has 40 % of Chile´s population, has reported high prevalence of malignant melanoma (Sabatini-Ugarte et al., 2018). Therefore, continuous monitoring of UVER and its corresponding UVI can provide useful information for risk assessment of skin and eye damage.

In the southern hemisphere, the increase of UVER irradiance is noteworthy (Corrêa, 2015), (Feng et al., 2015). Despite the expected increase in the stratospheric ozone content in next years (Hodzic and Madronich, 2018), the amount of UVER that reaches the surface needs to be considered due to its negative effects. However, measurements in spectral bands using ground-based instruments are scarce due to the instrumentation high cost and limiting studies about UVER, mainly in South America. One alternative, *that will be addressed in this work*, is using modelling techniques. There are UVER models based on numerical solution of the radiative transfer equations, such as TUV (Palancar et al., 2017), LibRadtran (Antón et al., 2012) and others (Koepke et al., 1998). They are difficult to use because they require a detailed description of the atmosphere composition, mainly ozone concentration, and of the thermodynamic state. There is a more simple model based only on empirical expressions derived from the correlation between solar global irradiance (IG) and its ultraviolet component, both measured independently at the surface (Ogunjobi and Kim, 2004), (Cañada et al., 2007), (Adam and Ahmed, 2016). Most of the correlation models reported in the literature were developed for measurements carried out in the northern hemisphere, for a variety of climatological conditions, e.g. in Kwangju, South Korea (Ogunjobi and Kim, 2004);

Selection and/or peer review under responsibility of Scientific Committee
doi:10.18086/swc.2019.45.04 Available at http://proceedings.ises.org

Valencia, Spain (Cañada et al., 2007); Wuhan, Central China (Wang et al., 2014); Qena, Egypt (Adam and Ahmed, 2016);, but stratospheric ozone spatial distribution differ from that in the southern hemisphere where fewer works are available as in Argentina (Salta, El Rosal, and Tolar Grande) (Utrillas et al., 2018) and Lauder, New Zealand (McKenzie et al., 2006).

Aiming to fill the observational gap, the main objective of the present work is to describe the seasonal variation of UVER radiation in Santiago de Chile, and derive a new empirical model to predict daily and hourly values of UVER from IG radiation at the surface that takes into consideration the climate conditions and air pollution effects of Santiago. This work is based on observation of UVER carried out in the urban area of Santiago continuously for four years, from 2015 to 2018. In this paper sections 1 and 2 show the introduction and methods and data. Section 3 describes seasonal variation of UVER. Section 4 describes the correlation model. Finally, section 5 summarizes the main findings of this research.

2. Methods and data

2.1 Site, climatology and sensors

Chile is a long and narrow country. It extends over 4,400 km in the longitudinal direction from 17°30′ S to 56º30′ S, displaying a variety of climatic conditions (Fig. 1a). The climate in northern Chile is characterized by high insolation due low cloudiness (Schulz et al., 2012). In the southernmost latitudes the increased cloudiness combined with astronomical factors reduce the incident solar radiation on the surface, mainly during the Austral winter. Santiago de Chile (33°30'S, 70°42'W), where this study is carried out, is a city with almost 6 million inhabitants (http://www.ine.cl) located at 88 km far from Pacific Ocean, in a relatively longitudinal valley at 520 m above sea level (asl) (Fig. 1c). The standard *Norma Chilena* (NCh 1079–2008) classifies Santiago´s climate as Mediterranean continental (Instituto Nacional de Normalización, 2008). Santiago's urban area is surrounded by a mountain range, with the Andean mountains (peaks 5 km) to the east and the coastal hills (peaks 1 km) to the west (Fig. 1c). These topographic features inhibit the air pollution dispersion and favors intense smog events in Santiago during the Austral winter (Morata et al., 2008).

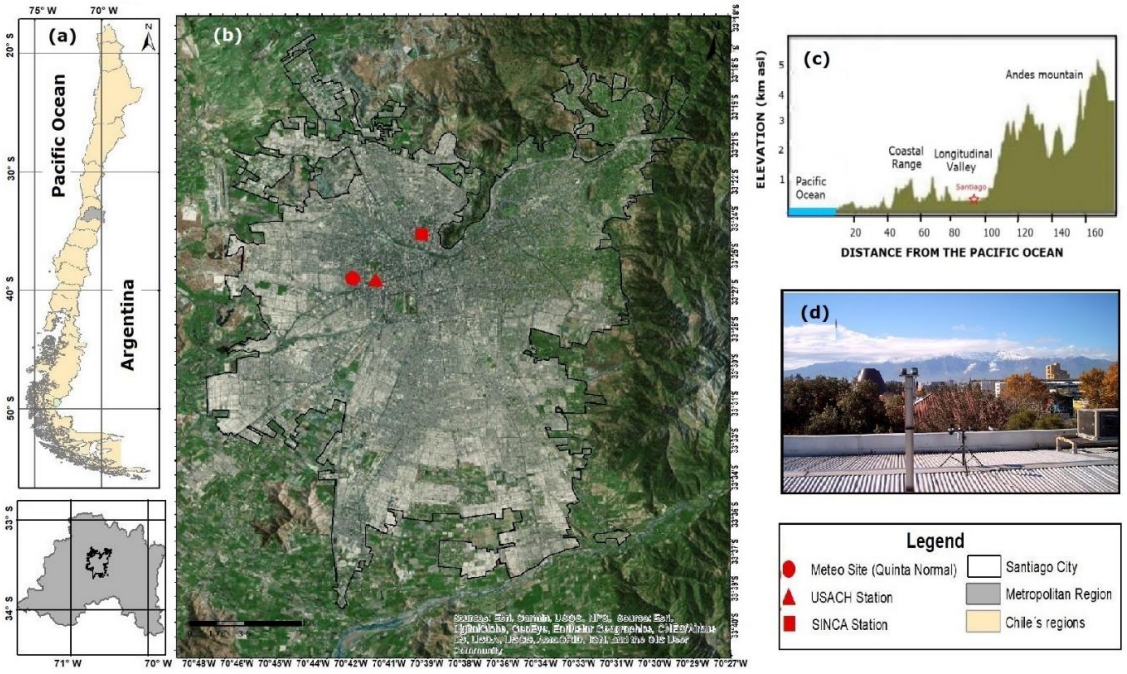

Figure 1. City of Santiago de Chile showing the location of the monitoring stations (a, b), elevation map (c) and sensors (d).

In this work, the UVER and IG were measured in the roof of 4-story building of the Physics Department (Fig. 1d) in the University of Santiago (USACH, "*Universidad de Santiago*") (33°27′24″S, 70°38′53″W, 512 m asl). The USACH is located in the Central Station district of the Metropolitan Region of Santiago and indicated in Fig. 1b (right panel). Hourly values of IG and UVER irradiances were measured with a pyranometer with photodiode model BPW46 and Analog Biologically Weighted Erythema UV-B Sensor; model PMA-1101 (Solar Light

Company, Inc.) respectively. These sensors are calibrated annually. Table 1 shows the main features of these sensors provided by the manufacturer. Note that the spectral ranges of pyranometer (350-1150 nm) and UV-B sensor (280-315 nm) do not overlap. For consistency values of UVER irradiance given in μWcm^{-1} are transformed to Wm^{-2}.

Table 1. Operational characteristics of solar sensors.

Features	IG	UVER
Manufacturer	Vishay Semiconductors	Solar Light Company, Inc.
Models	BPW46	PMA1101
Spectral Sensitivity	350 - 1150 nm	280 - 315 nm
Response time	10 min	2 min
Directional (Cosine) Response	± 65° zenith angle	5% for angles <60°
Operating Environment	-40 to +100°C	0 to +50°C
Units	Wm^{-2}	μWcm^{-2}

To complement the UVER analysis a set of meteorological (Air temperature, relative humidity, wind speed, precipitation and cloud cover) and environmental (particulate matter concentration and total ozone column) variables are used. These variables are analyzed by monthly mean values. Meteorological variables such as air temperature, relative humidity and precipitation were measured at the *Quinta Normal* station (33°26'27"S, 70°40'57"W, 520 m asl) belonging to the Chilean Meteorological Service (DMC, "*Dirección Meteorológica de Chile")* and indicated by *Quinta Normal* in Fig. 1b. In case, the relative humidity was taken the values at 08:00 local time (LT).

Particulate matter concentration for particles with radius smaller than 10 μm (PM_{10}), at surface (in $\mu g\ m^{-3}$), and wind speed at the reference level of 10 m above ground level (agl), were measured at *Independencia* station (33°25′00″S, 70°40′00″W, 536 m asl), belonging to the Air Quality Information System network (SINCA, "*Sistema de Información Nacional de Calidad del Aire"*) and indicated by SINCA in Fig. 1b. Data of Total Ozone Column (TOC) was obtained from measurements of the Ozone Monitoring Instrument–Total Ozone Mapping Spectrometer (OMI–TOMS) onboard NASA's Aura satellite available at NOAA Earth System Research Laboratory website. OMI-TOMS has a spatial resolution of 0.25 degree, which results in a ground resolution at nadir ranging from 13 km by 24 km to 13 km by 48 km. In addition, total cloud cover for the period 1983-2015, was taken from the International Satellite Cloud Climatology Project (ISCCP) (1-degree resolution) in the nearest grid point to Santiago de Chile.

2.2 Data quality control

A quality control procedure was applied to irradiances measurements where negative values and values higher than the Top-of-Atmosphere (TOA) were discard. The hourly values of UVER and IG irradiances at TOA are estimated using (1)-(3). The solar zenith angle (SZA) in (1) is estimated by the algorithm proposed by (Ibrahim Reda, 2004), the earth-sun distance factor (U) in (2) are based on the expression proposed by (Iqbal, 1983). Io is the extraterrestrial irradiance at 1 astronomical distance set equal to 1366 Wm^2 for IG and 9.89 Wm^{-2} for UVER (Utrillas et al., 2018). The yearlong variation of sun-earth relative position is indicated by (Γ) in (3) estimated in terms of the year day (Jday), vary from 1 on January 1 to 365 (366) on December 31(leap year).

$$I_{TOA} = I_0\ U\ cos\ SZA \tag{1}$$

$$U = 1.00011 + 0.034221\ cos\ \Gamma + 0.00128\ sin\ \Gamma + 0.000719\ cos\ 2\Gamma + 0.00007\ sin\ 2\Gamma \tag{2}$$

$$\Gamma = 2\pi \cdot (Jday - 1)/365 \quad (3)$$

After quality control, the resulting time series consist of 10,799 hourly values and 1,460 daily values for simultaneous measurements of UVER and IG. The available hourly values of solar irradiances are reprocessed into a daily and monthly resolution, respectively. Hourly values are expressed in irradiance units (Wm^{-2}) and daily values in irradiation units are expressed in kJm^{-2} for UVER and MJm^{-2} for IG, respectively. Table 2 shows the number measurements depending on the resolution at each year after the quality control.

Table 2. Number of values after the quality control.

Year	Hourly	Daily
2015	2,593	338
2016	3,022	351
2017	2,631	345
2018	2,533	332
Total	10,799	1,460

2.3 Models validation

A convenient measured of the correlation between two variables is the Pearson correlation coefficient (R) indicated (4), is a quantity that gives the quality of a least squares fitting. The R measures the direction of a relationship between two variables X and Y.

$$R = \frac{\sum_{i=1}^{N}(X_i - \bar{X})(Y_i - \bar{Y})}{\sqrt{\sum_{i=1}^{N}(X_i - \overline{X})^2}\sum_{i=1}^{N}(Y_i - \overline{Y})^2} \quad (4)$$

It should be noted that $-1 \leq R \leq +1$, where + and – signs are used for positive and negative correlations respectively. Where, $\bar{X}$ is the mean of X variable and $\bar{Y}$ mean of Y variable. When the value of the correlation coefficient (R) is multiplied by itself, R is squared (R^2). R^2 close to 1 indicates more efficient models. On the other hand, if there is no correlation, the R is close to 0. To verify the model performance a subset (10 %) of the data set described in Table 2 is removed from entire data set used to estimate the following statistical parameters: root mean square error (RMSE) indicated in (5) and normalized root mean square error (NRMSE) in (6) as indicated below:

$$RMSE = \left[\frac{\sum_{i=1}^{N}(P_i - O_i)^2}{N}\right]^{\frac{1}{2}} \quad (5)$$

$$NRMSE = \frac{RMSE}{\left(\frac{\sum_{i=1}^{N} O_i}{N}\right)} \quad (6)$$

Where P_i represents the modeled values and O_i the measured one, with N the number of observations. The RMSE is a frequently used to compare forecasting errors of different models (Despotovic et al., 2015). The NRMSE can be interpreted as a fraction of the mean error with respect to the average. In general, lower RMSE and NRMSE indicate better model performance.

3. Seasonal variation of UVER

3.1 Climate and environmental conditions

The seasonal variation of meteorological and environmental variables from 2015 to 2018 in Santiago are indicated in Fig. 2. During this period the mean temperature (relative humidity at 08:00 LT) is 15°C (78%), varying from minimum of 8°C (maximum of 94%) in the austral winter of 2017-2018 (2017) to a maximum of 24°C (minimum of 51%) in the austral summer of 2017 (Figs. 2a,b). Similarly, the mean wind speed is 1 m s^{-1}, varying from a minimum of 0.65 m s^{-1} in the austral winter of 2016 and a maximum of 1.39 m s^{-1} in the austral summer of 2017 (Fig. 2d). During this period, the prevailing wind direction is southwesterly (not show). The cloudiest period of the year begins in April and ends in October. Cloudy conditions predominate during 53% of the year. Comparatively, rainfall in Santiago presents larger interannual variability. The mean annual accumulated precipitation is 242 mm with a maximum of 111 mm in the austral winter of 2015 and no precipitation in the austral summer of 2016 (Fig. 2f). About 57% of the rainfall recorded in Santiago between 2015 and 2018 occurred from June to August. Considering period of observation from 1983 to 2015, the mean cloud cover is 67%, varying from a maximum of 79% in the austral winter (June) and a minimum of 52% the austral summer (January) (Fig. 2f). Based on analysis is possible to infer that mean conditions from 2015 and 2018 does not differ significantly from typical climate conditions in Santiago (Stolpe and Undurraga, 2016) and (Boisier et al., 2018).

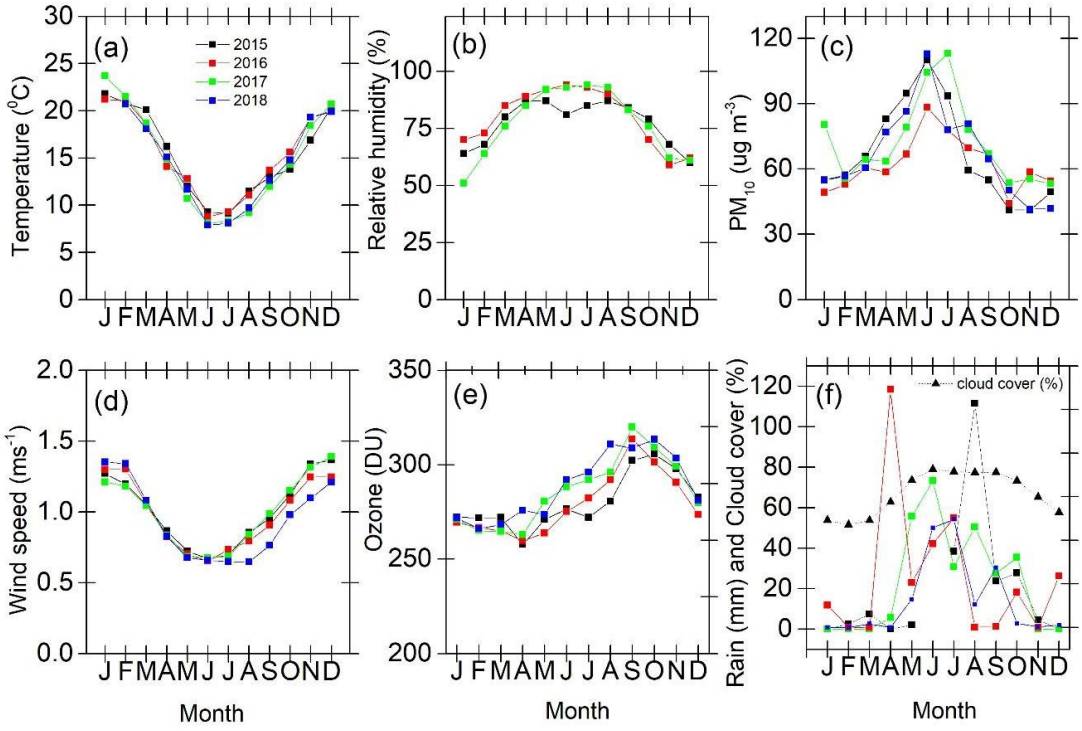

Figure 2. Annual variability the meteorological and environmental parameters available for Santiago, Chile.

From 2015 to 2018, the mean PM_{10} concentration in Santiago is 67 μg m^{-3}, varying from a maximum of 113 μg m^{-3} in the austral winter of 2017 to a minimum of 41μg m^{-3} in the austral summer of 2015 (Fig. 2c). In general, the geographic (Fig. 1) and climate (Fig. 2) conditions of the Santiago do not favor the dispersion of air pollutants. Especially during the winter months when low wind speed combined with shallow mixing layer height leads to high values of PM_{10} concentrations at the surface (Morata et al., 2008). Large concentration of aerosols during the winter in Santiago may affect the solar radiation field at the surface by increasing scattering and augmenting the diffuse component of global radiation detrimental to the direct beam component (Préndez et al., 1995). The large presence of aerosols during fog events in the winter in Santiago may affect also the spectral distribution of solar radiation, mainly in the UV bandwidth (Préndez et al., 1995), (Koronakis et al., 2002).

Similarly, during the period of 2015 and 2018, the mean TOC is 283 DU, varying from a minimum of 258 DU during the end of austral summer and begin of austral autumn of 2015 and a maximum of 320 DU in during the austral spring of 2017 (Fig. 2e). Compared to similar latitudes in the North Hemisphere mean TOC values in

Santiago is lower (Rafiq et al., 2017). Therefore, the seasonal evolution of TOC in Santiago indicates that steps should be taken to avoid overexposure to radiation UVER in the warmer months.

3.2 Annual cycle using daily values

Figure 3 displays seasonal evolution of statistical parameters based on charts plots of daily values UVER and IG observed in the Santiago from 2015 to 2018. The seasonal variation of mean values of UVER and IG are due mainly to astronomical factor. However, the seasonal variation of median, minimum value, maximum value, the 1st and 3rd quartiles and the 5th and 95th percentiles) may be strongly affected by the seasonal variation of climate (cloud, moisture) and environmental (TOC, PM_{10}) conditions (Fig 2).

The mean daily values of IG and UVER are 15.89 MJ m^{-2} and 2.93 KJ m^{-2}, respectively. Monthly average daily values of UVER vary from a minimum of 0.48 KJ m^{-2} in austral winter (June) to 5.99 KJ m^{-2} in the austral summer (December). The monthly average daily values of IG ranged from minimum of 6.52 MJ m^{-2} in the austral winter (July) to a maximum of 26.10 MJ m^{-2} in the austral summer (January). In case the UVER radiation, the absolute maximum of 7.86 KJ m^{-2} occurred during the austral summer (January) when TOC and cloud cover are minimum (Figs. 2 e,f).

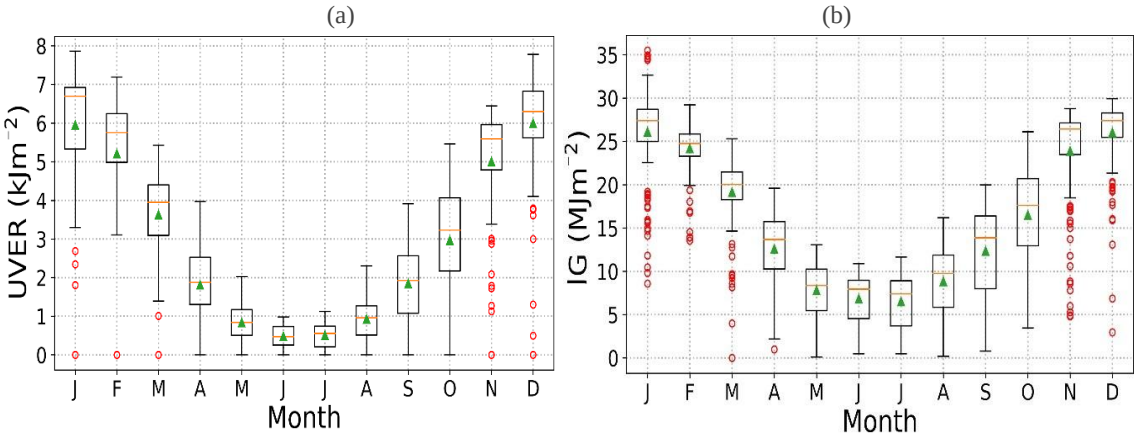

Figure 3. Seasonal variation of daily values of (a) UVER and (b) IG in Santiago de Chile. The boxplot extends from the percentile 25 to 75. Orange horizontal lines indicate the medians; green triangles indicate means and red circles outliers' values.

In contrast, the absolute minimum values of UVER (0 KJ m^{-2}) and IG (0.5 MJ m^{-2}) occurred during the austral winter months when cloud cover is maximum and TOC increases towards spring maximum (Figs. 2 e,f). During winter the air pollution conditions deteriorates in Santiago and the MP_{10} concentration (Fig. 2c) and other trace gases (nitrogen dioxide and sulfur dioxide) increases (Gallardo et al., 2002), attenuated the solar radiation beam and contributing to reduce UVER and IG at the surface. UV irradiances recorded under cloudy conditions can be enhanced by the radiation scattering, produces an effect in opposition to the attenuation events (Schwander et al., 2002).

Despite the astronomical, climatic and environmental conditions described in this section the observations carried out from 2015 to 2018 indicates that during eight months the hourly values of UVER at solar noon are systematically larger than 0.20 Wm^{-2}, indicating "very high" harmful potential according to the World Health Organization (WHO et al., 2002).

4. Correlation model

In the literature there are two types of correlation model for UVER: simple linear ($UVER = a_1\, IG + b_1$) and quadratic ($UVER = a_2\, IG^2 + b_2\, IG + c_2$) (Ogunjobi and Kim, 2004; Adam and Ahmed, 2016; Gholami and Yoosefi, 2009; Kudish and Evseev, 2000; Kudish and Evseev, 2011). The model type depends on shape of the experimental points distribution in the UVER-IG dispersion plot. In the case of Santiago, both hourly (Fig. 4a) and daily (Fig. 4b) UVER-IG dispersion plots indicate that the best fits are given by a second order polynomial for c_2 equal to zero. R^2 values higher than 0.90 (Fig. 4) confirmed the good correlation between UVER and IG.

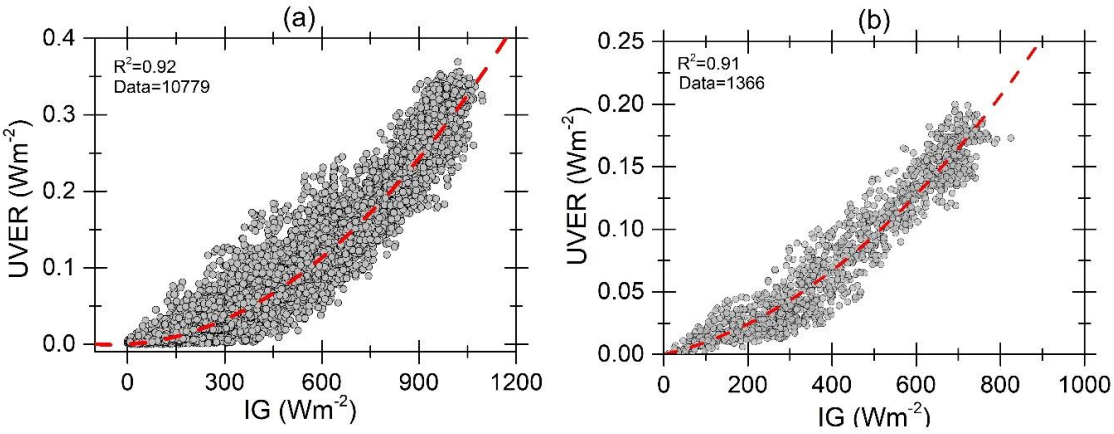

Figure 4. Scatter plot of (a) hourly and (b) daily UVER and IG in Santiago de Chile for all sky conditions.

Similar procedure was applied to subsets of the time series of hourly and daily values of UVER and IG for observations carried during summer, autumn, winter and spring months from 2015 and 2018. Tables 3-4 indicate second order polynomial coefficients and the statistical parameters RMSE and NRMSE considering the UVER model obtained for each season.

Table 3. The seasonal variation of regression equation coefficients and statistic parameters for empirical models of hourly values.

Season	a (10^{-7}) W^{-1} m^2	b (10^{-5})	RMSE	NRMSE	N
Summer	2.7	3.47	0.0279	0.2030	3860
Autumn	2.8	1.77	0.0187	0.2537	2307
Winter	1.4	4.47	0.0148	0.5351	1547
Spring	2.0	7.27	0.0296	0.3206	3065
Annual	2.2	5.18	0.0262	0.2751	10779

Table 4. The seasonal variation of regression equation coefficients and statistic parameters for empirical models of daily values.

Season	a (10^{-7}) W^{-1} m^2	b (10^{-5})	RMSE	NRMSE	N
Summer	-0.5	27.0	0.0147	0.0962	344
Autumn	1.7	9.80	0.0146	0.2382	340
Winter	-0.1	10.0	0.0076	0.3296	339
Spring	0.7	16.0	0.0152	0.1695	343
Annual	2.1	8.86	0.0174	0.2124	1366

In general, RMSE smaller than 0.03 Wm^{-2} for hourly (Table 3) and daily (Table 4) values of UVER, indicates that all models performed very well. In terms of NRMSE (percentage) the best performance is obtained during summer (20%) and the worst in the winter (53%) for hourly values of UVER. For daily values the model performed better during summer (9.6%) and worst during winter (32%). The performance reduction in the models during winter is caused by the increase in the cloud cover and aerosol loads in Santiago reduce the correlation between UVER and IG. Table 5 shows a comparison between UVER models available in the literature. The coefficients of model for hourly values in Santiago differ from ones obtained in Mediterranean sites in Cyprus (Kalogirou et al., 2017), indicating that correlation models for hourly values are strongly dependent on climate conditions and

environmental conditions.

Table 5. Regression equation coefficients and R^2 for empirical models of hourly values.

Site	Latitude, Longitude	Land use	Altitude (m asl)	a_2 (10^{-7}) W^{-1} m^2	b_2 (10^{-5})	R^2
Larnaca, Cyprus	34.87 N, 33.63 E	rural	1	1	17	0.96
Athalassa, Cyprus	35.14 N, 33.39 E	semi-rural	165	0.1	1.6	0.95
Santiago, Chile	33°30'S, 70°42'W	urban	520	2.2	5.8	0.92

5. Conclusion

In this work, four years of UVER measurements at the surface, carried out from January 1st, 2015 to December 31th, 2018, in Santiago City, Chile, are analyzed and used to develop a mathematical regression models to estimate hourly and daily values of UVER in terms of solar global irradiance (IG).
The UVER models, obtained by fitting a second-degree polynomial performed better during summer (RMSE=0.028, NRMSE=20%) and the worst in the winter (RMSE=0.015, NRMSE=54%) for hourly values. Similarly, performance is presented by daily values of UVER. In general, UVER can be estimated in terms of IG for Santiago using the following expressions:

$$UVER = 2.2*10^{-7}\ IG^2 + 5.18*10^{-5}\ IG \text{ (hourly)}$$

$$UVER = 2.1*10^{-7}\ IG^2 + 8.86*10^{-5}\ IG \text{ (daily)}$$

The results of this paper can be used in scientific areas such as solar climatology, photobiology, biophysical studies, and material degradation as well as in other scientific fields like water treatment in disinfection solar.

6. Acknowledgments

Thanks to: Professor Ernesto Gramsch for the effort to keep the National UV Measurement Network updated, University of Concepcion, Micrometeorology Laboratory, IAG-USP, Project Solar Energy Research Center, SERC-Chile (15110019) and Scholarship Nacional Doctorate CONICYT 2017.

7. References

Adam, M.E., Ahmed, E.A., 2016. An assessment of the ratio of ultraviolet-B to broadband solar radiation under all cloud conditions at a subtropical location. Adv. Sp. Res. 57, 764–775. doi:10.1016/j.asr.2015.11.030

Antón, M., Alados-Arboledas, L., Guerrero-Rascado, J.L., Costa, M.J., C Chiu, J., Olmo, F.J., 2012. Experimental and modeled UV erythemal irradiance under overcast conditions: The role of cloud optical depth. Atmos. Chem. Phys. 12, 11723–11732. doi:10.5194/acp-12-11723-2012

Boisier, J.P., Alvarez-Garreton, C., Cordero, R.R., Damiani, A., Gallardo, L., Garreaud, R.D., Lambert, F., Ramallo, C., Rojas, M., Rondanelli, R., 2018. Anthropogenic drying in central-southern Chile evidenced by long-term observations and climate model simulations. Elementa 6. doi:10.1525/elementa.328

Cañada, J., Esteve, A.R., Marín, M.J., Utrillas, M.P., Tena, F., Martinez-Lozano, 2007. Study of erythemal, UV (A+B) and global solar radiation in Valencia (Spain). Int. J. Clim. 416, 385–416. doi:10.1002/joc

Corrêa, M.D.P., 2015. Solar ultraviolet radiation: properties, characteristics and amounts observed in Brazil and South America. Contin. Med. Educ. 90, 297–310.

Despotovic, M., Nedic, V., Despotovic, D., Cvetanovic, S., 2015. Review and statistical analysis of different global solar radiation sunshine models. Renew. Sustain. Energy Rev. 52, 1869–1880. doi:10.1016/j.rser.2015.08.035

Escobedo, J.F., Gomes, E.N., Oliveira, A.P., Soares, J., 2009. Modeling hourly and daily fractions of UV, PAR and NIR to global solar radiation under various sky conditions at Botucatu, Brazil. Appl. Energy 86, 299–309. doi:10.1016/j.apenergy.2008.04.013

Feng, L., Wang, L., Gong, W., Lin, A., Hu, B., 2015. Estimation of hourly and daily ultraviolet solar irradiation under various sky conditions at Sanya, Southern China. Theor. Appl. Climatol. 121, 187–198. doi:10.1007/s00704-014-1239-3

Gallardo, L., Olivares, G., Langner, J., Aarhus, B., 2002. Coastal lows and sulfur air pollution in Central Chile. Atmos. Environ. 36, 3829–3841. doi:10.1016/S1352-2310(02)00285-6

Gholami, M., Yoosefi, L., 2009. Solar ultraviolet-B radiation monitoring in Khorram Abad City in Iran. Iran. J. Radiat. Res. 7, 171–175.

Hartman, R., Calvo, E., 2014. Cómo mejorar la prevención y detección del cáncer en Chile. Claves de Políticas Públicas 1–10.

Hodzic, A., Madronich, S., 2018. Response of surface ozone over the continental United States to UV radiation declines from the expected recovery of stratospheric ozone. Clim. Atmos. Sci. 1, 1–7. doi:10.1038/s41612-018-0045-5

Ibrahim Reda, A.A., 2004. "Solar position algorithm for solar radiation applications," Solar Energy. doi:doi:10.1016/j.solener.2003.12.003

Instituto Nacional de Normalización, 2008. NCh-1079-2008.

Iqbal, M., 1983. An Introduction to Solar Radiation., Academic P. ed.

Iribarren B., O., Ramírez S., M., Madariaga G., J.A., Riveros F., Ó., Valdés V., C., Toledo S., J., 2018. Carcinoma de células escamosas de piel. Serie de casos. Rev. Chil. cirugía 70, 315–321. doi:10.4067/s0718-40262018000300315

Kalogirou, S.A., Pashiardis, S., Pashiardi, A., 2017. Statistical analysis and inter-comparison of erythemal solar radiation for Athalassa and Larnaca, Cyprus. Renew. Energy 111, 580–597. doi:10.1016/j.renene.2017.04.043

Karimkhani, C., Green, A.C., Nijsten, T., Weinstock, M.A., Dellavalle, R.P., Naghavi, M., Fitzmaurice, C., 2017. The global burden of melanoma: results from the Global Burden of Disease Study 2015. Br. J. Dermatol. 177, 134–140. doi:10.1111/bjd.15510

Koepke, P., Bais, A., Balis, D., Buchwitz, M., De Backer, H., De Cabo, X., Eckert, P., Eriksen, P., Gillotay, D., Heikkilä, A., Koskela, T., Lapeta, B., Litynska, Z., Lorente, J., Mayer, B., Renaud, A., Ruggaber, A., Schauberger, G., Seckmeyer, G., Seifert, P., Schmalwieser, A., Schwander, H., Vanicek, K., Weber, M., 1998. Comparison of Models Used for UV Index Calculations. Photochem. Photobiol. 67, 657–662. doi:10.1111/j.1751-1097.1998.tb09109.x

Koronakis, P.S., Sfantos, G.K., Paliatsos, A.G., Kaldellis, J.K., Garofalakis, J.E., Koronaki, I.P., 2002. Interrelations of UV-global/global/diffuse solar irradiance components and UV-global attenuation on air pollution episode days in Athens, Greece. Atmos. Environ. 36, 3173–3181. doi:10.1016/S1352-2310(02)00233-9

Kudish, A.I., Evseev, E., 2000. STATISTICAL RELATIONSHIPS BETWEEN SOLAR UVB AND UVA RADIATION AND GLOBAL RADIATION MEASUREMENTS AT TWO SITES IN ISRAEL. Int. J. Climatol. 770, 759–770.

Kudish, A.I., Evseev, G., 2011. The analysis of solar UVB radiation as a function of solar global radiation , ozone layer thickness and aerosol optical density. Renew. Energy 36, 1854–1860. doi:10.1016/j.renene.2010.12.008

McKenzie, R., Bodeker, G., Scott, G., Slusser, J., Lantz, K., 2006. Geographical differences in erythemally-weighted UV measured at mid-latitude USDA sites. Photochem. Photobiol. Sci. 5, 343–352. doi:10.1039/b510943d

McKinlay, A.F. and Diffey, B.L., 1987. A Reference Action Spectrum for Ultraviolet Induced Erythema in Human Skin. CIE J. 6, 17–22.

Morata, D., Polvé, M., Valdés, A., Belmar, M., Dinator, M.I., Silva, M., Leiva, M.A., Aigouy, T., Morales, J.R., 2008. Characterisation of aerosol from Santiago, Chile: An integrated PIXE-SEM-EDX study. Environ. Geol. 56, 81–95. doi:10.1007/s00254-007-1141-8

Ogunjobi, K.O., Kim, Y.J., 2004. Ultraviolet (0.280-0.400 μm) and broadband solar hourly radiation at Kwangju, South Korea: Analysis of their correlation with aerosol optical depth and clearness index. Atmos. Res. 71, 193–214. doi:10.1016/j.atmosres.2004.05.001

Palancar, G.G., Olcese, L.E., Achad, M., Laura, M., Toselli, B.M., 2017. A long term study of the relations

between erythemal UV-B irradiance, total ozone column, and aerosol optical depth at central Argentina. J. Quant. Spectrosc. Radiat. Transf. 198, 40–47. doi:10.1016/j.jqsrt.2017.05.002

Préndez, M.M., Egido, M., Tomas, C., Seco, J., Calvo, A., Romero, H., 1995. Correlation between solar radiation and total syspended particulate matter in Santiago, Chile-Preliminary results. Atmos. Environ. 29, 1543–1551. doi:10.1016/1352-2310(94)00349-P

Rafiq, L., Tajbar, S., Manzoor, S., 2017. Long term temporal trends and spatial distribution of total ozone over Pakistan. Egypt. J. Remote Sens. Sp. Sci. 20, 295–301. doi:10.1016/j.ejrs.2017.05.002

Rivas, M., Rojas, E., 2018. Effects of ozone layer variation in Ultraviolet solar radiation level received at ground in Arica north of Chile. J. Phys. Conf. Ser. 1043. doi:10.1088/1742-6596/1043/1/012066

Rivas, M., Rojas, E., Calaf, G.M., 2014. Skin cancer risk affected by ultraviolet solar irradiance in Arica, Chile. Oncol. Lett. 7, 483–486. doi:10.3892/ol.2013.1698

Sabatini-Ugarte, N., Molgó, M., Vial, G., 2018. Melanoma en Chile ¿Cuál es nuestra realidad? Rev. Médica Clínica Las Condes 29, 468–476. doi:10.1016/j.rmclc.2018.06.006

Schulz, N., Boisier, J.P., Aceituno, P., 2012. Climate change along the arid coast of northern Chile. Int. J. Climatol. 32, 1803–1814. doi:10.1002/joc.2395

Schwander, H., Koepke, P., Kaifel, A., Seckmeyer, G., 2002. Modification of spectral UV irradiance by clouds. J. Geophys. Res. Atmos. 107, 1–12. doi:10.1029/2001JD001297

Stolpe, N., Undurraga, P., 2016. Long term climatic trends in Chile and effects on soil moisture and temperature regimes. Chil. J. Agric. Res. 76, 487–496. doi:10.4067/S0718-58392016000400013

Utrillas, M.P., Marín, M.J., Esteve, A.R., Salazar, G., Suárez, H., Gandía, S., Martínez-Lozano, J.A., 2018. Relationship between erythemal UV and broadband solar irradiation at high altitude in Northwestern Argentina. Energy 162, 136–147. doi:10.1016/j.energy.2018.08.021

Wang, L., Gong, W., Lin, A., Hu, B., 2014. Measurements and cloudiness influence on UV radiation in Central China. Int. J. Climatol. 34, 3417–3425. doi:10.1002/joc.3918

WHO, Meteorological, W., Programme, U.N.E., Protection, and the I.C. on N.-I.R., 2002. GLOBAL SOLAR UV INDEX A Practical Guide. Switzerland.